Atmospheric
Chemistry
and Physics
Discussions

Open Access

Quasi-biennial oscillation of the tropical stratospheric aerosol layer

R. Hommel[1],[*], C. Timmreck[1], M. A. Giorgetta[1], and H. F. Graf[2]

[1]Max Planck Institute of Meteorology, Hamburg, Germany
[2]Department of Geography, Centre for Atmospheric Science, Cambridge University, Cambridge, UK
[*]now at: Institute of Environmental Physics (IUP), University of Bremen, Bremen, Germany

Correspondence to: R. Hommel (rene.hommel@iup.physik.uni-bremen.de)

Discussion Paper | Discussion Paper | Discussion Paper | Discussion Paper

ACPD

14, 16243–16290, 2014

The QBO in tropical stratospheric aerosol

R. Hommel et al.

Title Page

Abstract | Introduction

Conclusions | References

Tables | Figures

◄◄ | ►►

◄ | ►

Back | Close

Full Screen / Esc

Printer-friendly Version

Interactive Discussion

Abstract

This study describes how aerosol in an aerosol-coupled climate model of the middle atmosphere is influenced by the quasi-biennial oscillation (QBO) during times when the stratosphere is largely unperturbed from volcanic material. In accordance with satellite observations, the tropical stratospheric aerosol load is predominately influenced by QBO induced anomalies in the vertical advection. Large impacts are seen in the size of aerosols, in particular in the region where aerosol evaporates. This turns the quasi-static balance between processes maintaining the vertical extent of the Junge layer in the tropics into a cyclic balance when considering this dominant mode of atmospheric variability. Global aerosol-interactive models without a QBO are only able to simulate the quasi-static balance state. To assess the global impact of stratospheric aerosols on climate processes, those partly non-linear relationships between the QBO and stratospheric aerosols have to be taken into account.

1 Introduction

The stratospheric aerosol layer, also referred to as the Junge layer (Junge et al., 1961), is a key constituent in the Earth's atmosphere. The Junge layer plays an important role in the determination of the Earth's radiation budget and interacts with the cycles of chemically-induced ozone depletion in the polar winter stratosphere. It is generally believed to be maintained by the oxidation of tropospheric Sulphur Dioxide (SO_2) and Carbonylsulphide (OCS), entering the stratosphere by troposphere–stratosphere-exchange processes (Holton et al., 1995; Fueglistaler et al., 2009), and by direct injections of volcanic material from modest to large volcanic eruptions (SPARC/ASAP, 2006; Bourassa et al., 2012). During times of low volcanic activity, the stratospheric aerosol load inevitably degrades towards a so called background state representing the lowest possible self-maintaining aerosol level in the stratosphere. However, this natural balance is influenced by sulphur releasing anthropogenic activities (Hofmann et al., 2009;

Neely et al., 2013). Together with the sporadically occurring volcanic perturbations, human activities alter the Earth's radiative balance, in turn affecting the long-term trend of the global aerosol load (Solomon et al., 2011). The relative contributions of the precursors to maintain the background Junge layer as well as their major pathways into the stratosphere (apart from direct injections by volcanoes) are not well understood (e.g. Hofmann, 1990; Hofmann et al., 2009; Deshler et al., 2006; SPARC/ASAP, 2006; Bourassa et al., 2012; Brühl et al., 2012; Rex et al., 2012; Neely et al., 2013).

With respect to the much-debated potential to moderate climate change by manipulating the Earth's albedo due to the enhancement of the stratospheric aerosol load, e.g. the Royal Society Report on Geoengineering the Climate (The Royal Society, 2009) explicitly emphasised a considerable demand to better understanding the spatio-temporal variability of the stratospheric aerosol system, including the barely explored coupling between the dynamics of the upper troposphere and lower stratosphere (UT/LS) and microphysical processes which are ultimately determining load, size and stability of this system. These problems are addressed in the current study.

A variety of fundamental questions of the stratospheric aerosol system have been addressed in the review of stratospheric aerosol processes by the WMO/SPARC initiative (SPARC/ASAP, 2006). It largely focussed on conditions observed after the powerful eruption of Mt. Pinatubo in 1991, which significantly influenced both the stratosphere and the Earth's climate in the subsequent two to three years. SPARC/ASAP (2006) also revealed a few remarkable scientific issues related to stratospheric background conditions. For instance, the report emphasised that measured LS aerosol quantities distinctly differ between the observational systems (in-situ, remote). More recent studies addressed this problem in several ways (e.g. Thomason et al., 2008; Damadeo et al., 2013) but since the decommissioning of the ERBS satellite in 2005, which hosted the SAGE II instrument, equivalently well examined data sets of vertically-resolved stratospheric aerosol size properties do not exist.

Another major uncertainty of the stratospheric aerosol system arises from the lack of observations of the precursors SO_2 and H_2SO_4 vapour in the stratosphere. SO_2

and H_2SO_4 vapour quantities have not yet been systematically monitored in the LS – contrary to the troposphere, in particular the boundary layer. Only a few individual measurements of the two gases were conducted in the stratosphere during balloon ascents in the nineteen-seventies and -eighties (see Hommel et al., 2011, herein referred to as HOM11, for a review). Only a single remotely sensed SO_2 profile existed for altitudes above 30 km, obtained during a NASA Space Shuttle mission in 1986 (Rinsland et al., 1995), until very recently a new SO_2 data set has been derived from Envisat/MIPAS observations (Höpfner et al., 2013).

With respect to modelling initiatives aiming to better understand the stratospheric aerosol-climate system, there has also scarcely been any progress since SPARC/ASAP (2006) emphasised distinct differences between modelled aerosol quantities and observations. Most studies of global climate models with interactively coupled aerosol size and microphysics schemes focus on the examination of the tropospheric aerosol-climate system, predominately detached from stratospheric aerosol processes (Ghan and Schwartz, 2007; IPCC, 2013). Only a very limited number of studies addressed aerosol processes in the UT/LS by means of aerosol size resolving microphysics models that have been interactively coupled to global climate models. Some studies focussed on the determination of aerosol induced climate effects of the Mt. Pinatubo eruption 1991 (Niemeier et al., 2009). Other studies investigated the stability of the Junge layer during the stratospheric background periods (Timmreck, 2001; Pitari et al., 2002; Hommel et al., 2011; English et al., 2011; Brühl et al., 2012).

In this study we address the coupling between the stratospheric dynamics and aerosol microphysical processes, whose understanding is key to evaluate stratospheric geoengineering options. We focus on effects imposed by the quasi-biennial oscillation (QBO) in the tropical stratosphere (reviewed in Baldwin et al., 2001) as this dominant mode of stratospheric variability largely impacts the global dispersion of stratospheric trace constituents (e.g. Gray and Chipperfield, 1990). We elaborate a numerical experiment to simulate an 11 yr stratospheric background period after 1995, when the stratosphere had recovered from the violent eruption of Mt. Pinatubo in June 1991

(SPARC/ASAP, 2006). This is done by coupling an aerosol size resolving microphysics scheme (SAM2; HOM11) and a middle-atmosphere circulation model (MAECHAM5; Manzini et al., 2006) that precisely specifies the QBO (Giorgetta and Bengtsson, 1999). To avoid any interference with effects superimposed from other external sources, the model is driven in a climatological mean configuration and does not consider any volcanic or pyro-cumulonimbus injections into the stratosphere. The analysis focus on the spatio-temporal evolution of the Junge layer in the tropics, because the QBO signature is strongest in the equatorial belt. Modelled aerosols do not radiatively feed back to the general circulation and the QBO, neither directly nor by impacting the stratospheric ozone chemistry. Both may be important in particular for the extra-tropics and are in the scope of following studies.

Although stratospheric aerosols have been monitored with sufficient global coverage since the end of the seventies, QBO signatures in observed post-Pinatubo stratospheric background aerosol quantities have only been inferred in a very limited number of studies (Choi et al., 1998, 2002; Barnes and Hofmann, 2001). Since these studies do not show QBO signatures in other aerosol quantities than the retrieved extinction coefficients or the aerosol backscatter, in this study we also infer QBO signatures from climatologies of the aerosol surface area density and the aerosol effective radius, both inferred from SAGE II retrieved extinction coefficients, in order to establish a direct comparison between our modelled aerosol properties and observations.

The paper is structured as follows: first we give a brief overview about the model used in this study. The following sections describe the influence of the QBO on a variety of modelled aerosol parameters in the equatorial stratosphere and compare the results to other data from observations or models. The final section summarises our findings.

The QBO in tropical stratospheric aerosol

R. Hommel et al.

Title Page

Abstract	Introduction
Conclusions	References
Tables	Figures

⏮ ⏭

◀ ▶

Back Close

Full Screen / Esc

Printer-friendly Version

Interactive Discussion

2   Methodology

2.1   Model framework

The model framework used to assess the interannual variability of the aerosol layer in the tropical stratosphere during times of stratospheric background is identical to the model described in detail in HOM11. In this study a middle-atmosphere general circulation model with an interactive, particle size-resolved aerosol dynamics module was evaluated against satellite data and in-situ observations. The major difference between the companion study of HOM11 and this work is the representation of the quasi-biennial oscillation in the equatorial stratosphere. While our applied model setup has no internally generated QBO (Giorgetta et al., 2002, 2006), we perform an additional experiment in which the QBO is nudged towards observed winds from radiosonde measurements at Singapore (updated from Naujokat, 1986) by applying the method of Giorgetta and Bengtsson (1999). Hereafter, comparisons between the two model setups are referred to as CTL (control run) for the free running model of HOM11, and QBO for the QBO-nudged simulation. For details on the host model and the aerosol dynamics scheme we refer the reader to HOM11 – in the following only the basic features needed to understand the experimental set up are described.

The model was integrated in T42 truncation, using an associated grid with a horizontal resolution of about $2.8° \times 2.8°$. In the vertical, 39 sigma-hybrid layers resolved the atmosphere up to 0.01 hPa (~ 80 km) with a layer thickness increasing from about 1.5 km to 2 km in the region of the tropical Junge layer. Around the stratopause, the layer thickness is about 3 km, further increasing towards the model's top of atmosphere to ~ 6.5 km (Giorgetta et al., 2006, their Fig. 1). The time integration interval was 15 min. In the QBO configuration, the modelled zonal wind in the equatorial stratosphere is nudged towards the zonal wind profile observed at Singapore (see Giorgetta and Bengtsson, 1999), assuming a Gaussian latitudinal distribution of the zonal wind about the equator with a half width increasing from 7° at 70 hPa to 10° at 10 hPa. The nudging rate is 1/(10 days) between 70 hPa and 10 hPa and between 10° N and 10° S.

Poleward of 10° latitude the nudging rate is linearly reduced to zero at 20° latitude. Outside of this region the zonal wind remains unaffected by the nudging scheme.

To ensure that the model's interannual variability is unaffected by the prescribed boundary conditions, we applied perpetual monthly climatologies of AMIP2 sea surface temperatures and sea ice concentrations as lower boundary conditions. Natural and anthropogenic sulphur emissions were taken from the AeroCom database (scenario B) and represent year 2000 conditions (Dentener et al., 2006).

In the microphysics scheme SAM2 (HOM11), aerosols are resolved throughout the atmosphere in 35 logarithmically spaced bins that range from 1 nm to 2.6 µm in radius. For the sake of computational efficiency aerosols are assumed to be composed of a binary H_2O–H_2SO_4 mixture, which is a reasonable assumption under stratospheric conditions (e.g. Hamill et al., 1997). Microphysical processes considered are binary homogeneous nucleation (BHN; Vehkamäki et al., 2002), condensation and evaporation of water and sulphuric acid, as well as Brownian coagulation and gravitational sedimentation. In the troposphere, aerosol washout processes and surface deposition are treated as in Stier et al. (2005). Aerosols are advected segment-wise employing a semi-Lagrangian advection scheme (Lin and Rood, 1996) in terms of their mixing ratio relative to the mass of sulphur (S) incorporated in the droplets.

Similar to HOM11, the model applies an offline chemistry scheme based on prescribed climatological monthly zonal mean oxidant fields of OH, O_3, NO_2, H_2O_2. Also OCS mixing ratios are prescribed. The aerosol radiative effects follows the ECHAM5 standard approach and rely on emissivities obtained from the Tanre et al. climatology (see Roeckner et al., 2003). Interactions between aerosols and the cycles that form and maintain high altitude clouds (cirrus and polar stratospheric clouds) have not been considered.

The model was run over 17 years, from January 1990 to December 2006. Only the last 11 years were analysed (1996–2006). Hommel (2008) showed that the model reaches a steady state of the stratospheric aerosol layer after six years. Then no fur-

ther impact from the initialisation of the model was detectable for any of the aerosol parameters.

2.2 Observational aerosol data

For comparison, we use the aerosol forcings data set compiled for the WMO/SPARC Chemistry Climate Model Initiative (CCMI; http://www.pa.op.dlr.de/CCMI). This data set provides consistent aerosol forcings for the troposphere and stratosphere up to 39.5 km ($\sim$ 3 hPa). For the stratospheric background period between 1996 and 2006, this gridded and gap filled data set combines observations from the satellite instruments ERBS/SAGE II (1996–May 2005) and Calipso/CALIOP (June 2005–December 2006). Aerosol surface area densities (SAD) were derived from SAGE II (vn7) size distribution fits to measured aerosol extinction coefficients in four wave-lengths as described in Arfeuille et al. (2013). This method takes the composition of aerosol droplets (weight percentage) into account, as determined by stratospheric temperature and water content of the ECMWF ERA-Interim reanalysis. CALIOP SAD were obtained from a conversion of the measured aerosol backscatter into extinction coefficients at 532 nm wave-length and a subsequent fit of uni-modal log-normal distributions based on SAGE II extinction correlations (Beiping Luo, ETH, personal communication, July 2013).

In relation to the SADs of the predecessor initiative CCMVal (Chemistry-Climate Model Validation Activity) forcing data set (http://www.pa.op.dlr.de/CCMVal/Forcings/CCMVal_Forcings_WMO2010.html), the newer data provide a much better representation of aerosols in the post-Pinatubo stratospheric background period. Beyond 2004 CCMVal SADs were represented as recurring 5 yr-averages from 1998 to 2002, that erase any information about the QBO-Junge layer relationship in the equatorial stratosphere from the data and largely impact the derivation of anomalies from the long-term average.

A comparison to other data sets and gridded climatologies of aerosol size properties is not possible at this point, because those either cover a few years of the post-Pinatubo stratospheric background only (Bauman et al., 2003a, b; Wurl et al., 2010) or contain

to many gaps (SPARC/ASAP, 2006; Wurl et al., 2010), which makes a statistically meaningful calculation of residual anomalies impossible.

2.3 Meteorology

The model's ability to adequately reproduce the QBO through the nudging procedure is assessed by comparison to the ECMWF ERA-Interim reanalysis. Figure 1 compares the temporal development of the ERA-Interim zonal mean zonal wind at the equator from 1996 to 2006 (Fig. 1a) to the two model configurations (Fig. 1b and c). Through QBO-nudging the temporal behaviour of alternating zonal mean zonal winds in the model applied in this study is well reproduced (Fig. 1b), whereas in the free-running model (CTL) easterly winds prevail in the lower tropical stratosphere throughout the year (Fig. 1c). Also the onset of the descent of the QBO above 10 hPa is adequately reproduced in the nudged model, although in this region no nudging was performed.

Figure 2 shows associated temperature anomalies in the equatorial stratosphere that are imposed by the QBO to maintain the thermal wind balance. The QBO signature is expressed in this figure as a residual anomaly, composited relative to the time of wind shear onset at 18 hPa (reanalysis at 20 hPa). The reanalysis (Fig. 2a) is 3 to 4 K colder around 10 hPa during times of easterly shear and 2 K warmer during westerly shear between 50 and 30 hPa than the QBO nudged model (Fig. 2b). The model shows somewhat stronger anomalies above 10 hPa. As the climatologies of the equatorial zonal winds differ between the QBO and CTL experiments, also the temperature profiles differ (Fig. 2c). In the QBO simulation the QBO easterlies and westerlies dominate in the upper and lower stratosphere, respectively, thus create a time mean vertical shear that results in temperature anomaly profile that is negative in the middle stratosphere and positive above the tropopause and below the stratopause, compared to the case of the CTL simulation with very weak wind shear in the climatological mean. Thus, in the time mean the CTL simulation has colder tropical tropopause layer (TTL) conditions than the more realistic QBO simulation with an imposed QBO. This also affects the mean tropical upwelling that is reduced by approximately one half between 70 hPa

and 50 hPa in the nudged model, and improves the representation of the water vapour tape recorder (Giorgetta et al., 2006).

From Fig. 1 it is obvious that only the model which represents the QBO realistically describes the variability in the equatorial stratosphere. This may have implications for thermodynamic properties of aerosols in this region and for the processes that form and maintain the aerosol layer.

3 Results and discussion

Observational evidence that the QBO affects the stratospheric aerosol layer came from aerosol extinctions measurements in the early years of systematically monitoring the stratosphere from space (e.g. Trepte and Hitchman, 1992; Grant et al., 1996). In an aerosol-coupled chemistry climate model simulation, Brühl et al. (2012) reproduced the temporal development of the tropical aerosol mixing ratio that has been inferred from SAGE II extinction measurements. But their time-slice experiment was conducted for 33 months during a period of low volcanic activity in the stratosphere between January 1999 and September 2002, that only covers a single QBO cycle. In the following, the influence of the QBO on the modelled aerosol mixing ratio is examined and their influence on other parameters describing the aerosol population in the stratosphere are investigated. Conclusively, QBO signals in precursors are examined and implications for aerosol formation and growth are given.

3.1 Aerosol mixing ratio

3.1.1 Temporal evolution

The configuration of the model in HOM11 did not allow to consider QBO effects on stratospheric trace constituents. Therefore, in the HOM11 study, the Junge layer behaves almost statically, in the tropics only being influenced by temperature variations in

the TTL and wind alterations related to the semi-annual oscillation (SAO) in the meso-sphere and upper stratosphere (Fig. 3a; see also Giorgetta et al., 2006). Figure 3b shows the strong variability in the temporal evolution of the modelled aerosol mixing ratio in the equatorial lower stratosphere of the QBO nudged experiment.

Without QBO, anomalies in the aerosol mixing ratio, relative to the climatological mean annual cycle, appear like the tape recorder signal (not shown) in tropical strato-spheric water vapour (Mote et al., 1996). In contrast, the interannual variability of the tropical aerosol layer in the QBO-nudged experiment is much stronger and depends on the strength and direction of the zonal winds in the equatorial stratosphere. The QBO directly influences the vertical extent of the layer and modulates the peak aerosol mixing ratio in the tropical stratospheric reservoir (TSR; Trepte and Hitchman, 1992) by about 5 %, relative to the CTL simulation, with larger values seen during times of maximum easterly wind acceleration.

The characteristic patterns of upward and downward motion of the tropical Junge layer result from a superposition of advection by the extra-topically driven Brewer–Dobson circulation (BDC), the meridional circulation imposed by the QBO (also known as the secondary meridional circulation, SMC, or residual circulation of the QBO), and the annual cycle in the tropopause temperature. The thermal wind relationship requires that westerly zonal wind shear is balanced by warm anomalies. This causes a descent of equatorial air relative to the tropical upwelling that is associated with the BDC. Con-sequently, easterly zonal wind shear is balanced by cold anomalies and induced rel-ative ascent. The associated meridional circulation is characterised by anti-correlated upward (downward) motion in the extra-tropics at levels of QBO westerly (easterly) shear, and meridional convergence (divergence) in the QBO westerly (easterly) jet. Hence, advective effects of the secondary circulation of the QBO on the QBO jets contributes to narrower (in latitude) and deeper westerly jets compared to wider and shallower easterly jets. Due to this secondary circulation also the tropical reservoir that is confined by the sub-tropical mixing-barrier (e.g. Grant et al., 1996) expands merid-ionally (horizontal divergence) during the time of maximum easterly zonal wind accel-

eration and appears compacted in the vertical (vertical convergence). The opposite is the case during times of maximum westerly zonal wind acceleration: the tropical stratosphere is narrowed in the horizontal and stretched in the vertical. Those structures are easily inferable from concentration gradients of stratospheric trace constituents. A re-

5 spective model goes back to the works of Plumb and Bell (1982), for TSR aerosol it was first reported by Trepte and Hitchman (1992) based on aerosol extinction measurements from SAGE I and II instruments in the periods 1979–1981 and 1984–1991, when the volcanic aerosol load of the stratosphere was relatively low. Underlying mechanisms were later examined in detail by Choi et al. (1998) and Choi et al. (2002) from

10 HALOE observations of aerosol extinction, ozone and other trace gases.

These relationships are responsible for the characteristic temporal evolution of the simulated Junge layer in the tropics: as seen in Fig. 3b, the largest vertical expansion of the Junge layer slightly lags behind the occurrence of strongest QBO westerlies at 30–20 hPa. And the largest reduction in the vertical extent is found after QBO easterlies

15 were strongest above 20 hPa. This vertical spread of the layer is accompanied with an increase in its top height, that varies from around 10 hPa during times of the onset of westerly winds and $\sim$ 6 hPa in the aftermath of the easterly QBO shear. This increase in top height is more distinct at lower altitudes where the layer is denser, i.e. between 20 and 10 hPa. For instance, in this region the 0.35 ppbm mixing ratio isopleth steeply

20 raises vertically after westerlies were strongest. A large lofting of particulate material is also found in the lower regions of the layer, that, moreover, outweigh displacements at its top edge. Bottom displacements are in the order of 3–5 km, whereas the layer's top drifts no more than 2–3 km.

It is nicely seen in Fig. 3b that after the layer reaches its largest vertical expansion,

25 the model predicts that the entire layer descends under the influence of descending easterly zonal winds. As mentioned above, this descent is in the order of 2–3 km around the onset of the westerly wind shear around the 15 hPa pressure level. This settling is accompanied by the above mentioned horizontal divergence of the TSR, which shifts the subtropical mixing barriers a few degrees poleward (Grant et al., 1996; Neu et al.,

2003). The net change of this variation, that is the difference in the layer thickness due to the QBO, is at least 5 km.

Since this spatio-temporal structure of TSR aerosols is intrinsically linked to circulation patterns superimposed by the QBO in the tropical upwelling branch of the BDC, the model predicts that the SMC stabilise the Junge layer at higher altitudes, where in the QBO-free model of HOM11 aerosols are no longer thermodynamically stable. Mechanisms that act in particular on the top lid of the layer are discussed in greater detail in Sect. 3.4.

3.1.2 QBO induces anomalies in the tropical mixing ratio

To gain further insight into QBO effects on the dynamics of aerosols in the tropical lower stratosphere, in the following (Figs. 4–11), we discuss simulated anomalies induced by the QBO in aerosol mixing ratio and other LS aerosol properties. All data are zonal means and have been averaged between 5° N and 5° S. Profile data are climatological means of the analysed period. Composites of residual QBO anomalies, relative to the time of the onset of westerly zonal mean zonal wind at 18 hPa, were obtained from monthly means.

Figure 4a shows the climatological averaged aerosol mixing ratio profile. Respective residual anomalies induced by the QBO are shown in Fig. 4b. Largest modulations are found in the regions of large vertical gradients, especially in the upper levels near 7 to 10 hPa, where sulphate droplets evaporate. During QBO east phase, the bulk mixing ratio increases in this region by about 60 %. In the QBO westerly shear and during the QBO westerly phase a decrease relative to the mean annual cycle of 60–90 % is found. In contrast, around 20 hPa, where the bulk mixing ratio is largest, and below, in regions where the mixing ratio gradient is positive, only very moderate QBO modulations of less than ±5 % are found.

A phase reversal in the sign of the anomalies is seen along the isopleths of descending zonal mean zonal winds around the 20 hPa pressure level, where the aerosol mixing ratio is largest. Very similar anomalies are induced by the QBO in tropical stratospheric

ozone. Ozone anomalies show a phase reversal around 10 hPa that corresponds to the altitude of maximum ozone mixing ratio in the equatorial stratosphere (Hasebe, 1994; Butchart et al., 2003). This phase reversal results from QBO modulations in the vertical advection as discussed above. Negative anomalies are produced in the westerly shear, where the vertical mixing ratio gradient is negative above 20 hPa, and positive anomalies where the gradient is positive below 20 hPa (Choi et al., 2002).

Ozone anomalies at the equator are reported to be in the order of 3 to 15 % (e.g. Butchart et al., 2003), hence are of similar strength as the QBO related aerosol variability in regions where the mixing ratio gradient is positive (below 20 hPa). Above, in the evaporation region, the aerosol QBO is quite stronger with relative modulations that exceed 50 %. This implies that QBO modulations in the aerosol transport alone cannot explain this behaviour. Therefore, it is reasonable to assume that QBO modulates microphysical processes as well, in particular the process of aerosol evaporation in higher altitudes (Sect. 3.4).

Despite the similarities between the QBOs in ozone and aerosol in the tropical lower stratosphere, there is a distinct difference between them: the thermodynamic limitation of the stability of liquid-phase aerosols in the LS imposes a characteristic oscillating temporal behaviour on the upper edge of the tropical Junge layer (nicely seen in the mixing ratio time-series Fig. 3b), which is not known from the ozone layer in the tropical stratosphere. Implications for the size of aerosols and processes that maintain them are discussed in the following sections.

3.2 Integrated aerosol size parameters

3.2.1 Surface area density

Integrated aerosol parameters, inferred from observed aerosol extinction coefficients at specific wave length, are fraught with uncertainties when the fraction of small particles significantly contributes to an aerosol size distribution (Dubovik et al., 2000; Thomason et al., 2008). In particular, this becomes important when the aerosol load of the strato-

sphere is low (SPARC/ASAP, 2006). HOM11 showed that integrated aerosol parameters of the CTL simulation vary considerably if the aerosol distribution is determined by condensational growth. It is therefore important to take this into account when modelled aerosol sizes are compared with observed data.

The SAD from the model simulation strongly depends on the size-range of the integration (Fig. 5a and c). The climatological mean SAD profile decreases with height, which results from persistent changes in the size spectrum of the particles: at lower levels, larger particles are more abundant than in the upper layers. This has two reasons: first, when particles grow, they are also removed quicker. A similar effect occurs when particles of a given size are advected into higher altitudes because their sedimentation velocity increases with height. Secondly, at higher altitudes the saturation vapour pressure of H_2SO_4 at the surface of the aerosol droplet increases so that the particles also evaporate quicker. Whereby larger aerosol particles evaporate at higher rates than smaller particles. Hence, with increasing altitude the size distribution of a stratospheric aerosol population is always shifted towards the fine mode.

Compared to the CTL simulation, with a more or less static tropical Junge layer, the QBO nudged version shows 6 % lower SADs throughout the year between 80 hPa and 20 hPa. In contrast, directly above the TTL SADs are larger by 4–6 % in the QBO model and up to 30 % larger above the 10 hPa pressure level, where evaporation is strong.

The climatological mean SAD (Fig. 5c) has a distinct different shape than the integral of the entire size spectrum (Fig. 5a), if one considers only aerosol sizes that are detectable by satellite-sensors (particle radii < 0.005 μm). The SAD increases from the TTL to 70 hPa, where its maximum value is around 15 % smaller. Here, the modelled aerosol spectrum is dominated by small, newly formed aerosols (HOM11), which would not be seen by the satellite-sensor. The effect on the QBO modulations inferred from the SAD integrals is shown in Fig. 5b and d. QBO anomalies themselves as well as their phase transitions between the lower and upper parts of the Junge layer are more pronounced in the SAD inferred from the entire aerosol spectrum. The relative strength

The QBO in tropical stratospheric aerosol

R. Hommel et al.

of the QBO effects in the two SAD integrals, however, does not differ much below the 20 hPa pressure level and is in the order of ±5 %, relative to the absolute value.

This is different in the upper levels of the Junge layer: above 20 hPa relative SAD QBO modulations may exceed ±100 %, although absolute values here are more than one order of magnitude smaller than in regions of the layer further below. Those large modulations can be explained by QBO modulations in the reversible mass transfer of sulphuric acid vapour. In regions where warm (cold) anomalies are induced by the QBO in westerly (easterly) shear, the QBO fosters evaporation (condensation) and the SAD will be smaller (larger). In Sect. 3.4 we examine this relationship in more detail. Also here in the evaporation region, there is almost no difference deducible in the relative strength of the modulations between the two SAD integrals.

The surface area density derived from satellite observations is substantially smaller compared to the model as shown in Fig. 6a for the two SAD data sets compiled for the WMO/SPARC initiatives CCMI and CCMVal as prescribed forcings for CCMs. Both data sets are based on SAGE II aerosol extinction observations (vn7 and vn6.2 of the operational NASA retrieval). HOM11 found a similar difference to SAGE II climatologies in a comparison of the modelled SAD of the CTL configuration with the retrieved SAD climatologies of Bauman et al. (2003a, b) and Wurl et al. (2010). This agrees furthermore with SPARC/ASAP (2006), that revealed a significantly positively biased SAD (factor 2 to 10) in the tropical LS for the majority of models that participated in an intercomparison, compared to the operational vn6.2 SAGE II SAD.

Below the 30 hPa pressure level, the climatological mean tropical profile of the CCMI SAD forcing data set is about 30 % smaller than in the CCMVal SAD forcing data set. Above $\sim$ 15 hPa the CCMI SAD forcing is distinctly larger with values above $0.3\,\mu m^2\,cm^{-3}$, whereas, in contrast, the CCMVal SAD forcing tend to be zero. The latter indeed agrees better to our QBO and CTL simulations, where above 15 hPa the aerosols begin to evaporate and substantially shrink in size, which imposes a net loss in mass and also in the aerosol's number density.

Although the climatological mean values of the CCMI SAD forcing data set at the equator are smaller than in our model simulations, observed QBO induced anomalies (Fig. 6b) agree to a certain extent with our model predictions. Generally, the amplitudes of the inferred anomalies are similar, although they are slightly larger in CCMI between the TTL and about 40 hPa. The largest differences are found in the regions where the QBO westerly zonal wind is strongest between 50 and 20 hPa. In contrast, above 20 hPa QBO anomalies are in good agreement. It is likely that most of the somewhat irregularly appearing anomalies in the CCMI forcing data set below the 40 hPa pressure level reflect the release of volcanic material into the lower tropical stratosphere. Several moderate volcanic eruptions occurred in the later years of the analysed period (tropical volcano eruptions of Ruang occurred in late 2002, Manam in January 2005, Soufriere Hills in May 2006 and Tavurvur in October 2006) and are suspected to have dispensed sufficient amounts of precursors in the tropical LS, that quickly formed new aerosols (Vernier et al., 2011; Neely et al., 2013).

3.2.2   Effective radius

The aerosol effective radius (R_{eff}) is another key parameter widely used in the determination of UTLS aerosol climate effects (e.g. Grainger et al., 1995). Although negatively biased to observations, in the control experiment without a QBO the model predicted R_{eff} lies within the uncertainty range of the measurements (HOM11). Compared to the CTL experiment, the climatological mean tropical R_{eff} profile in the QBO experiment (Fig. 7a) shows 1–2.5 % smaller values, except in the lowest regions, between the TTL and 70 hPa, where it is about 2 % larger.

In Fig. 7b QBO induced R_{eff} anomalies are shown for aerosols larger than 50 nm in radius to ensure comparability with the particle sizes seen by remote sensing instruments. Although the patterns of QBO anomalies indicate strong modulations in R_{eff} except in the region between 20–10 hPa, their relative strength is significant only above 10 hPa, where the size of evaporating aerosols rapidly decreases with increasing altitude. Here, QBO related anomalies reach 60 % and are rather in-phase with anomalies

in the mixing-ratio (Fig. 4b) than with anomalies in the SAD (Fig. 5b). Below 20 hPa, QBO induced modulations are smaller than ±5 %, which is weaker than in the SAD.

No QBO signature would be seen in R_{eff} if the QBO affects the aerosol volume distribution and surface distribution in an equal measure. This is quite interesting in so far as HOM11 pointed out that most of the differences between the model R_{eff} and observational estimates can be assigned to invariable moments of the modelled aerosol populations (the relative position between volume and surface distribution in the model does not vary much in the stratosphere). In reality, the different moments seem to be much more variable (bottom panel of Fig. 9 in HOM11), and QBO nudging apparently helps to improve the model results.

3.3 Number density

In previous sections, QBO effects on integrated aerosol quantities were examined. In the following we further investigate how the QBO affects the size of aerosols in the tropical LS by an analysis of anomalies induced in specific ranges of their size distribution. Therefore, the modelled size distribution is partitioned into four size ranges, equivalent to the four modes, which are commonly used to define an aerosol distribution (e.g. Seinfeld and Pandis, 2006). In this respect, nucleation mode aerosols refer to particles with radii smaller than 0.005 μm. The Aitken mode is defined as the range between 0.005 μm and below 0.05 μm and the accumulation mode between 0.05 μm and below 0.5 μm. The coarse mode considers aerosols with radii equal or larger than 0.5 μm.

Figure 8 shows that QBO modulations strongly differ in the four modes. This was implicitly expressed also in Fig. 5 by the small differences in the anomalies in SAD for the two integration ranges (whole spectrum and aerosols larger than 50 nm). In contrast to SAD anomalies, relative QBO effects in aerosol number densities are much stronger.

Strong positive modulations, i.e. increased number densities, are seen in the larger three modes of the size distribution (Fig. 8d, f and h) during easterly QBO phases and above regions where the largest bulk mixing ratios are found (30–20 hPa). Anomalies

in the coarse mode number density (Fig. 8h) appear somewhat irregularly in the lowest levels above the TTL. Here QBO effects infer with effects imposed by the annual cycle in the tropical tropopause, which has no definite synchronisation with the QBO phase (Baldwin et al., 2001). Above 70 hPa, coarse mode number density anomalies are positive during the time when easterly zonal wind prevails and may reach 100 % in the evaporation region due to the low abundance of aerosol coarse mode particles there (Fig. 8g).

Alterations in the accumulation mode number density (Fig. 8c) are mainly confined to regions where the droplets evaporate and get smaller. In contrast to the coarse mode, from the climatological mean profile (Fig. 8e) it is obvious that at those altitudes accumulation mode particles are relatively abundant, although at least one order of magnitude less than further below, where the bulk mixing ratio is largest (Fig. 4a). In the latter region, i.e. between 50 and 20 hPa, relative modulations are below ±5 % all the way down to the TTL.

In the tropical LS, the Aitken mode aerosol concentration is largest just above the TTL, and rapidly decreases with increasing height (Fig. 8c). Collisional scavenging (coagulation) is responsible for the concentration decrease in the lower region of the layer, up to 30 hPa, while evaporation is a sink for both aerosol mass and number density above 20 hPa. Relative QBO modulations in the Aitken mode number density are quite strong throughout the entire tropical Junge layer. Modulations of ±20 % are found between 50 and 30 hPa and reach 100 % in the evaporation region. That is in contrast to the other modes, the mixing ratio and the SAD, where strong relative modulations are confined to the upper regions of the layer (above 30 hPa). In addition, also the characteristic patterns of positive/negative anomalies and their phase reversal in the vertical make this particular QBO effect exceptional in comparison to the other analysed QBO effects on tropical LS aerosols. This result clearly indicates that QBO effects on aerosol processes in the tropical LS interact highly nonlinearly with each other.

As seen from the nucleation mode number density profile (Fig. 8a), binary homogeneous nucleation (BHN) can occur in the tropical LS. Below 50 hPa, several hundred

The QBO in tropical stratospheric aerosol

R. Hommel et al.

|◄ | ►|

◄ | ►

Back | Close

Full Screen / Esc

Printer-friendly Version

Interactive Discussion

Discussion Paper | Discussion Paper | Discussion Paper | Discussion Paper

Full Screen / Esc

Printer-friendly Version

Interactive Discussion

nucleation mode aerosols are found per cm^{-3} in the model. Above 50 hPa, their number density rapidly decreases and is almost three orders of magnitude lower around 20 hPa and above. Since the BHN parametrisation depends on the ambient temperature and water vapour content, it is not surprising that the QBO may influence the particle forma-
5   tion process, and this is presumably reflected here in the quite strong modulations of nucleation mode number densities (Fig. 8b). The anomalies are confined mainly to the region between 70 and 30 hPa. Above this layer, the higher stratospheric temperature and lower moisture content more and more inhibit BHN. However, small fluctuations are even seen above 30 hPa, that indicate either rapid vertical transport of freshly formed
10   nuclei is imposing those signatures or even in the central and upper regions of the Junge layer nucleation is triggered by QBO imposed temperature fluctuations on rel-atively short time-scales. We will further examine those relationships in Sect. 3.4. As a caveat it should be mentioned that in particular the nucleation process of aerosols is poorly understood. Therefore, the above relationships strongly rely on the assumptions
15   we made in modelling the process and for the composition and size of nucleation mode aerosols in the LS.

3.4   Microphysical processes

To reveal the mechanisms responsible for the QBO effects discussed above, we fur-ther examine how microphysical processes are affected by the QBO. Principally, the
20   strength of aerosol microphysical processes depends on the thermodynamic state of the stratosphere. Temperature and the vapour contents of water and sulphuric acid de-termine the rate of formation of new aerosol, their growth and loss through reversible mass transfer between the gas and the liquid phase. Here, we do not consider aerosol growth by coagulation nor particle sedimentation since these processes have not been
25   diagnosed from the model in a manner that would allow an examination of QBO signa-tures.

3.4.1 Nucleation

In the lower tropical stratosphere, the modelled BHN rate after Vehkamäki et al. (2002), exhibits a maximum at 50 hPa (Fig. 9a). Above 50 hPa, it rapidly declines and tends to zero at 30 hPa as in the CTL run (HOM11). The pattern of QBO induced anomalies in the aerosol nucleation rate (Fig. 9b) correlates well with the QBO signature in the nucleation mode number density (Fig. 8b). The cold anomaly at QBO east shear imposes a 5–10 % amplification of the BHN rate around the 50 hPa pressure level. Although this is not a large number, the respective increase in the nucleation mode number density can amount to 50 %. At 30 hPa and above no significant impact of the QBO on the BHN is found, so that respective signatures seen in the nucleation mode number density (Fig. 8b), as discussed in Sect. 3.3, may have a different origin than new particle formation. QBO effects in the lowest regions of the LS strongly interfere with seasonal variations in the TTL, so that the composite of QBO signatures in the BHN rate appears rather irregularly.

3.4.2 Condensation of H_2SO_4

Following the approach of HOM11, we analyse QBO signatures in condensation and evaporation of aerosols in terms of a time-averaged H_2SO_4 molecule concentration that is transferred between the gas and the liquid phase.

Below 50 hPa, the model indicates that H_2SO_4 condensation is quite strong, but it decreases rapidly with height as seen from the climatological mean profile of H_2SO_4 molecules that condenses onto aerosols (Fig. 9c). The respective QBO signature (Fig. 9d) shows three regimes that are out of phase in the upper and lower regions of the Junge layer. Phase reversals occur around 15 hPa and between 7 and 5 hPa.

When easterly winds prevail at 50 hPa or below, positive anomalies in the condensational growth in the order of 5–10 % are induced by the QBO. Here, QBO induced cold anomalies in the stratospheric temperature (Fig. 2b) reduce the saturation vapour pressure of H_2SO_4 at the droplet surface that fosters condensation. Since in these regions

the total aerosol number concentration is much larger than above, the aerosol provides a large surface area for condensing molecules (Fig. 5a), and is therefore a strong sink for the H_2SO_4 vapour.

However, relative QBO anomalies are much larger (about ±60 %) in regions of the Junge layer where aerosols predominately release their mass into the gas phase, i.e. above 20 hPa (Fig. 9e). This indicates that both processes occur simultaneously in the time mean, and there is no sharp transition identifiable between regions where aerosols predominantly grow or shrink. Here, above 20 hPa, the reversible mass transfer of H_2SO_4 molecules is in a cyclic balance that depends on the strong in-phase relationship between the QBO modulated stratospheric temperature and the H_2SO_4 vapour pressure. QBO modulated upwelling through the tropical tropopause (Gray and Chipperfield, 1990; Seol and Yamazaki, 1998) may additionally contribute to QBO signatures in H_2SO_4 condensation and are further discussed in Sect. 3.6.

In the regions of the Junge layer where the mixing ratio and the number densities of intermediate size aerosol are sufficiently large, i.e. below 10 hPa, the QBO signatures of H_2SO_4 condensation correspond well with those in the Aitken mode number density (Fig. 8d). At certain levels they also correspond with the signatures in the number densities of the accumulation mode (between 50 and 30 hPa) and the coarse mode (between the TTL and 70 hPa).

3.4.3 Evaporation of H_2SO_4

Above 20 hPa, the H_2SO_4 saturation vapour pressure at the surface of the droplets gets larger than the H_2SO_4 partial pressure due to the photochemical production of H_2SO_4, so that aerosols evaporate quicker than at lower altitudes. The process reaches its maximum strength around 7 to 5 hPa (Fig. 9e). Above that level, most of the sulphate mass remains in the vapour phase and evaporation from aerosols strongly decreases.

Due to the strong in-phase relationship between the H_2SO_4 vapour pressure and the QBO temperature signature, evaporation anomalies are also in phase with temperature anomalies imposed by the QBO. The model indicates that during the warm

anomaly QBO westerly shear the process is fostered, while cold anomalies in the QBO easterly shear have a dampening effect. Figure 9d and f imply that the two intrinsically competing processes condensation and evaporation apparently occur simultaneously. This mainly arises from the time-averaging (composited monthly means) of the two unidirectional flows, directed either into the gas phase or onto the aerosols.

As mentioned before, the tropical Junge layer has a much larger variability in the QBO-nudged simulation than in the CTL simulation. In the QBO experiment, the balance in the mass transfer is shifted towards evaporation above 10 hPa. Although evaporation impose a decrease in the SAD (the total number of aerosols remains constant when they evaporate or even decreases due to complete evaporation) that is compensated in the QBO experiment by the QBO modulation of the advection of small aerosols. This results in a positively modulated SAD in the QBO easterly shear above 10 hPa (Fig. 5).

It should be mentioned, that compared to the ERA-Interim reanalysis, modelled QBO temperature anomalies are up to 2 K smaller below the 10 hPa pressure level (Fig. 2a and b) and 1–2 K larger above 10 hPa, where evaporation occurs. Thus, in the model the net effect of QBO on the evaporation of sulphate droplets may be overestimated to some degree.

3.5 Particle properties

Aerosols in the stratosphere become more concentrated with height until the increase in the H_2SO_4 saturation vapour pressure at the surface of the droplet sets an upper limit to the thermodynamic stability of the droplets. The concentration change of the droplet solution is obvious from the climatological mean tropical profiles of the binary solution density (Fig. 10a), the sulphuric acid weight percentage of the droplets (Fig. 10c), and their water content (Fig. 10e). The latter is expressed as the relative difference to a representative Junge layer aerosol mean state as it is widely used in literature (density of 1.7 g cm^{-3}, sulphuric acid weight percentage of 0.75; see e.g. Rosen, 1971; Hamill et al., 1997).

Changes in the aerosol composition play an important role for understanding seasonal variations of observed aerosol optical properties (e.g. Yue et al., 1994; Hamill et al., 1997). Since equilibrium with respect to water is achieved quasi-instantaneously also in the relatively dry stratosphere, small variations in the water content forced by the QBO may additionally contribute to QBO signatures in the droplet composition that arise from QBO induced temperature anomalies or advection due to the residual circulation of the QBO.

Residual QBO anomalies of the diagnosed particle properties (Fig. 10b, d and f) indeed reveal a strong analogy to QBO induced temperature anomalies of the tropical stratosphere (Fig. 2b). Aerosols have a higher sulphuric acid weight percentage during times when positive temperature anomalies are induced during the QBO westerly shear. Although respective relative modulations almost linearly scale with the QBO temperature signal, in the order of approximately ±1 %, this has extensive consequences for aerosol microphysics above the 20 hPa pressure level because it facilitates evaporation and reduces the SAD. The opposite occurs in the relatively cold QBO east shear.

In the lower regions, where evaporation is negligible and the mixing ratio is much larger, i.e. below 20 hPa, this QBO effect interferes with effects imposed by the annual cycle in the modelled stratospheric temperature. During the summer months, when the temperature in the upwelling branch of the BDC increases by 2–6 K, relative to winter conditions, sulphate droplets maintain their equilibrium with the ambient air through the release of H_2O and H_2SO_4 molecules so that they get smaller (Steele and Hamill, 1981).

3.6 Precursor gases

Previous work already addressed some aspects of the natural variability of aerosol precursors in the stratosphere. HOM11, for example, discussed in detail how the QBO-free model predicts the aerosol precursors SO_2 and sulphuric acid vapour in the stratospheric background in comparison to observations. Brühl et al. (2012) analysed the

modelled short term variability of SO_2 and sulphuric acid vapour with respect to oxidising capabilities of OCS in the volcanically quiescent stratosphere from 1999 and 2002. But Brühl et al. (2012) did not in greater detail investigate the coupling between the aerosol layer, the precursors and the QBO.

Generally, little is known about the vertical profiles of SO_2 and H_2SO_4 vapour in the stratosphere. Most measurements were conducted in the early years of systematic exploration of the stratosphere (SPARC/ASAP, 2006; Mills et al., 2005; HOM11). During the last two decades the majority of observations of sulphur bearing gases were conducted in the troposphere. According to SPARC/ASAP (2006) less than a quarter of the campaigns measured in the lowermost stratosphere. In the more recent years, SO_2 measurements were conducted on a more regularly base, e.g. when aircraft campaigns touched the lowermost stratosphere (e.g. during SOLVE). But those are predominately confined to the lowermost regions of the mid- and high latitudes, so that they cannot be taken into consideration within this study that focus on the tropical LS. Above 30 km data from only one campaign was available until last year (2013) that measured SO_2 in the NH subtropics (ATMOS infrared spectrometer on a NASA Space Shuttle in 1985; Rinsland et al., 1995). Recently a climatology of monthly and zonal mean profiles of SO_2 volume mixing ratios has been derived from Envisat/MIPAS measurements in the altitude range 15–45 km for the period from July 2002 to April 2012 (Höpfner et al., 2013). Only a few extra-tropical data are available for H_2SO_4 vapour and are discussed in Mills et al. (2005) and HOM11.

In the model, the climatological mean SO_2 mixing ratio rapidly decreases from the TTL to ~ 50 hPa due to rapid photochemical conversion to H_2SO_4 (Fig. 11a). Above 50 hPa, the mixing ratio increases due to the oxidation of OCS. Above 10 hPa the photolysis of H_2SO_4 vapour establishes an upper-stratospheric reservoir of SO_2, which plays a large role in the triggering of new aerosol formation in the polar spring stratosphere when the sunlight returns (Mills et al., 1999, 2005, HOM11).

The modelled climatological mean tropical H_2SO_4 vapour mixing ratio profile (Fig. 11c) exhibits a minimum slightly above the 50 hPa pressure level, where the

vapour rapidly condenses onto aerosols. Above 50 hPa, the saturation vapour pressure of H_2SO_4 rapidly increases (between 50 and 10 hPa by 7 orders of magnitude) so that with increasing altitude less vapour condenses and most of it remains in the gas phase. Above 20 hPa, the probability of droplet evaporation gradually increases with height, so that the gradient in the sulphuric acid vapour mixing ratio further increases to around the 5 hPa level. That is the altitude where H_2SO_4 photolysis to SO_3 becomes important (Burkholder and McKeen, 1997). SO_3 in turn is photolysed to SO_2 and builds up the SO_2 reservoir in the upper stratosphere. This is seen in most of the stratosphere-resolving (chemistry-) climate models with an interactive aerosol component (Turco et al., 1979; Weisenstein et al., 1997; Mills et al., 2005; HOM11). Envisat/MIPAS observations recently confirmed the existence of such a reservoir (Höpfner et al., 2013), that has been already indicated by ATMOS measurements in spring 1985 at northern hemispheric subtropical latitudes. Above 45 km, however, the ATMOS profile implies a further sink for SO_2 near the stratopause by largely decreasing mixing ratios above 48 km ($\sim$ 1 hPa), that is not confirmed by most models.

As seen from Fig. 11b and d, the QBO similarly modulates to a large degree SO_2 and H_2SO_4 vapour in the equatorial stratosphere. Just above the TTL we found deviations from the climatological mean of up to ±20 %. Above 20 hPa, the relative QBO signature may reach ±50 %. While below 50 hPa, positive (negative) anomalies correlate with easterly (westerly) winds, the anomalies above relate to the QBO shear, hence, are in-phase with the QBO temperature signal. A phase shift in the anomalies is found at approximately 10 hPa in SO_2 and in H_2SO_4 vapour around the 3 hPa pressure level. Höpfner et al. (2013) report QBO signatures in MIPAS observed SO_2 of 15–20 pptv between 30 and 37 km altitude at the equator between 10° S–10° N, that is 30–50 % of the observed climatological means.

Below the QBO easterly jet upwelling is enhanced (Gray and Chipperfield, 1990; Seol and Yamazaki, 1998), hence positive precursor anomalies below 50 hPa pressure level reflect enhanced vertical transport through the TTL in the model. To what extent H_2SO_4 vapour is transported from the free troposphere into the LS remains specula-

tive, because the small chemical time constant of H_2SO_4 vapour in the LS (~ 1 day) implies that H_2SO_4 vapour anomalies may appear as finger-print structures of the SO_2 anomalies. This is also supported by the kinetics of the H_2SO_4 vapour forming reaction between SO_3 (oxidised from SO_2) and H_2O, that depend exponentially on $1/T$ (Sander et al., 2006), hence benefit from cold anomalies induced in the cold lowermost tropical stratosphere during QBO east phases.

Above 50 hPa, where modelled anomalies in both gases correlate well with the equatorial QBO temperature signal, it seems plausible that some of the H_2SO_4 vapour anomalies arise implicitly from the QBO modulated SO_2 oxidation. Phase reversal of the anomalies occur where the mixing ratio profile distinctly changes shape, thus indicate that QBO modulated advective transport accounts for most of the calculated QBO anomalies in the two precursor gases.

Furthermore, modelled QBO anomalies in the two precursor gases are in-phase with modulations in the Aitken mode aerosol number density (Fig. 8d) and the H_2SO_4 vapour that condenses onto aerosols (Fig. 9d). This implies that pre-existent or newly formed aerosols rapidly grow by H_2SO_4 condensation, even though the strength of condensation decreases rapidly with height (Fig. 9c). Together with in-phase anomalies in the nucleation rate and nucleation mode number density around 50 hPa, this indicates that to a certain extent the origin of Aitken mode aerosols in the LS is not the free troposphere, from where they have been more rapidly uplifted when the QBO phase is easterly.

4 Conclusions

Here, for the first time, we provide model-based indications for concurrent QBO imposed effects in the tropical stratospheric aerosol layer that shape the aerosol size distribution in a highly nonlinearly manner. Such effects have only been suggested so far from satellite-measured aerosol extinction coefficients (Trepte and Hitchman, 1992). Eleven years (1996–2006) of the post-Pinatubo stratospheric background were

simulated with the aerosol-coupled middle-atmosphere circulation model MAECHAM5-SAM2. The data were examined with regard to the long-term variability of aerosol and precursors in the tropical lower stratosphere and variations caused by the QBO in aerosol dynamics and composition. We compared the data to a control simulation that did not resolve the QBO (HOM11), and to merged data sets from observations of the solar occultation SAGE II satellite sensor and the spaceborne CALIOP lidar.

There is a general agreement that the QBO is an important forcing mechanism of the Earth's climate (e.g. Baldwin et al., 2001; Brönnimann, 2007) and largely determines the global dispersion of stratospheric trace constituents (see Baldwin et al., 2001). However, accompanying effects on sulphate aerosol droplets that form the Junge layer in the stratosphere have not yet been addressed in detail. In this paper, we have shown that in the model the tropical Junge layer is heavily influenced by the QBO. The vertical expansion of the modelled layer, i.e. its thickness, differs by at least 5 km dependent on the phase of the QBO. This is in agreement with satellite observed aerosol extinctions and derived aerosol sizes, hence, does not arise solely from volcanic disturbances of the tropical lower stratosphere as argued by Hasebe (1994). This is important for understanding the climatological relevance of stratospheric background aerosols, which is still debated (e.g. Hofmann, 1990; Deshler et al., 2006; Solomon et al., 2011; Neely et al., 2013).

We found that the QBO affects all parameters we diagnosed from the model's aerosol scheme. Our results indicate that QBO effects in the sulphate droplet composition are rather small and depend almost linearly on the QBO signature in the tropical stratospheric temperature. QBO modulations in the modelled aerosol mixing ratio and size appear to be stronger and increase in the upper levels of the Junge layer (above 20 hPa), where the droplets evaporate. In particular at these altitudes we found clear indications for non-linear relationships in the aerosol processing due to the influence of the QBO. Furthermore, and in agreement with other studies, we found an enhanced upwelling of SO_2 into the lower stratosphere below the 50 hPa pressure level when the QBO is in its east phase. Our model indicates that this modulation in the supply of the

SO$_2$ precursor establishes a chain of subsequent in-phase modulations in other modelled quantities below 50 hPa. The sulphuric acid vapour concentration is enhanced during easterly QBO and also the subsequent condensation onto intermediate sized aerosols in the Aitken mode.

Compared to the CTL experiment, where the Junge layer behaves almost statically, the nature of the more realistically predicted Junge layer in the QBO experiment is predicted to be highly variable. Prevailing westerly zonal winds expand the layer in the vertical. This motion subsequently is backed by an adiabatically uplift of aerosols in the anomalously cold QBO easterly shear. With progressing downward motion of descending easterly zonal winds, the entire layer descends and vertically diverges due to advection imposed by the QBO meridional circulation overlying the BDC. Before the QBO westerly jet propagates through the layer, reduced upwelling below the jet is further displacing the layer down to lower altitudes, where the layer has its smallest vertical extension.

Resulting anomalies in the modelled tropical aerosol mixing ratio are very similar to those observed in ozone, hence are dominated by QBO effects on the advective transport and are confined by the structure of the mixing ratio profile in the tropics and exhibit a positive gradient above the TTL and a negative gradient above the mixing ratio maximum. In the upper levels of the Junge layer, integrated aerosol size quantities are much stronger modulated by the QBO than the bulk mixing ratio because imposed effects on microphysical processes play a larger role than further below. The model predicts that the QBO modulates also the balance of H$_2$SO$_4$ between the gas and the droplet's liquid phase. Mass transfer is shifted towards evaporation in the QBO nudged model, compared to the CTL simulation. However, in the time average, evaporation is continuously accompanied by recurring condensation of H$_2$SO$_4$ onto the aerosols. The model indicates that below the evaporation region nucleation of particles is triggered by the QBO and may significantly influence the aerosol size distribution. However, this result strongly relies on use of the Vehkamäki-parametrisation of binary homogeneous nucleation of the sulphuric acid-water mixture in the model. QBO effects on the extra-

tropical Junge layer were not at the scope of this study. Further investigations follow to examine respective relationships.

The complexity of the described interactions between the QBO and the Junge layer in the model might be a key aspect in attempts to understand the global impact of strato-spheric aerosols. It may also help to assess the discrepancy between modelled and observed aerosol quantities in periods when the stratosphere is largely unperturbed by sporadic injections from volcanoes or other sources. Although not addressable with this model configuration, the catalytic cycles that destroy wintertime polar stratospheric ozone may respond to QBO effects in the Junge layer. And, moreover, it seems likely that such effects may feed back into the climate system, further complicating the comprehensive understanding of the aerosol system in the UTLS.

References

Arfeuille, F., Luo, B. P., Heckendorn, P., Weisenstein, D., Sheng, J. X., Rozanov, E., Schraner, M., Brönnimann, S., Thomason, L. W., and Peter, T.: Modeling the stratospheric warming following the Mt. Pinatubo eruption: uncertainties in aerosol extinctions, Atmos. Chem. Phys., 13, 11221–11234, doi:10.5194/acp-13-11221-2013, 2013. 16250

Baldwin, M. P., Gray, L. J., Dunkerton, T. J., Hamilton, K., Haynes, P. H., Randel, W. J., Holton, J. R., Alexander, M. J., Hirota, I., Horinouchi, T., Jones, D. B. A., Kinnersley, J. S.,

Marquardt, C., Sato, K., and Takahashi, M.: The quasi-biennial oscillation, Rev. Geophys., 39, 179–229, 2001. 16246, 16261, 16270

Barnes, J. E. and Hofmann, D. J.: Variability in the stratospheric background aerosol over Mauna Loa observatory, Geophys. Res. Lett., 28, 2895–2898, 2001. 16247

5 Bauman, J. J., Russell, P. B., Geller, M. A., and Hamill, P.: A stratospheric aerosol climatology from SAGE II and CLAES measurements: 1. Methodology, J. Geophys. Res., 108, 4382, doi:10.1029/2002JD002992, 2003a. 16250, 16258

Bauman, J. J., Russell, P. B., Geller, M. A., and Hamill, P.: A stratospheric aerosol climatology from SAGE II and CLAES measurements: 2. Results and comparisons, 1984–1999, J.
10 Geophys. Res., 108, 4383, doi:10.1029/2002JD002993, 2003b. 16250, 16258

Bourassa, A. E., Robock, A., Randel, W. J., Deshler, T., Rieger, L. A., Lloyd, N. D., Llewellyn, E. J. T., and Degenstein, D. A.: Large volcanic aerosol load in the stratosphere linked to asian monsoon transport, Science, 337, 78–81, doi:10.1126/science.1219371, 2012. 16244, 16245

15 Brönnimann, S.: The impact of El Niño-Southern Oscillation on European climate, Rev. Geophys., 45, RG3003, doi:10.1029/2006RG000199, 2007. 16270

Brühl, C., Lelieveld, J., Crutzen, P. J., and Tost, H.: The role of carbonyl sulphide as a source of stratospheric sulphate aerosol and its impact on climate, Atmos. Chem. Phys., 12, 1239–1253, doi:10.5194/acp-12-1239-2012, 2012. 16245, 16246, 16252, 16266, 16267

20 Burkholder, J. B. and McKeen, S.: UV absorption cross sections for SO_3, Geophys. Res. Lett., 24, 3201–3204, 1997. 16268

Butchart, N., Scaife, A. A., Austin, J., Hare, S. H. E., and Knigh, J. R.: Quasi-biennial oscillation in ozone in a coupled chemistry–climate model, J. Geophys. Res., 108, 4486, doi:10.1029/2002JD003004, 2003. 16256

25 Choi, W., Grant, W. B., Park, J. H., Lee, K., Lee, H., and Russell III, J. M.: Role of the quasi-biennial oscillation in the transport of aerosols from the tropical stratospheric reservoir to midlatitudes, J. Geophys. Res., 103, 6033–6042, 1998. 16247, 16254

Choi, W., Lee, H., Grant, W. B., Park, J. H., Holton, J. R., Lee, K.-M., and Naujokat, B.: On the secondary meridional circulation associated with the quasi-biennial oscillation, Tellus B, 54,
30 395–406, 2002. 16247, 16254, 16256

Damadeo, R. P., Zawodny, J. M., Thomason, L. W., and Iyer, N.: SAGE version 7.0 algorithm: application to SAGE II, Atmos. Meas. Tech. Discuss., 6, 5101–5171, doi:10.5194/amtd-6-5101-2013, 2013. 16245

Dentener, F., Kinne, S., Bond, T., Boucher, O., Cofala, J., Generoso, S., Ginoux, P., Gong, S., Hoelzemann, J. J., Ito, A., Marelli, L., Penner, J. E., Putaud, J.-P., Textor, C., Schulz, M., van der Werf, G. R., and Wilson, J.: Emissions of primary aerosol and precursor gases in the years 2000 and 1750 prescribed data-sets for AeroCom, Atmos. Chem. Phys., 6, 4321–4344, doi:10.5194/acp-6-4321-2006, 2006. 16249

Deshler, T., Anderson-Sprecher, R., Jäger, H., Barnes, J., Hofmann, D. J., Clemesha, B., Simonich, D., Osborn, M., Grainger, R. G., and Godin-Beekmann, S.: Trends in the nonvolcanic component of stratospheric aerosol over the period 1971–2004, J. Geophys. Res., 111, D01201, doi:10.1029/2005JD006089, 2006. 16245, 16270

Dubovik, O., Smirnov, A., Holben, B. N., King, M. D., Kaufman, Y. J., Eck, T. F., and Slutsker, I.: Accuracy assessments of aerosol optical properties retrieved from Aerosol Robotic Network (AERONET) Sun and sky radiance measurements, J. Geophys. Res., 105, 9791–9806, 2000. 16256

English, J. M., Toon, O. B., Mills, M. J., and Yu, F.: Microphysical simulations of new particle formation in the upper troposphere and lower stratosphere, Atmos. Chem. Phys., 11, 9303–9322, doi:10.5194/acp-11-9303-2011, 2011. 16246

Fueglistaler, S., Dessler, A. E., Dunkerton, T. J., Folkins, I., Fu, Q., and Mote, P. W.: Tropical tropopause layer., Rev. Geophys., 47, RG1004, doi:10.1029/2008RG000267, 2009. 16244

Ghan, S. J. and Schwartz, S. E.: Aerosol properties and processes: a path from field and laboratory measurements to global climate models, B. Am. Meteorol. Soc., 88, 1059–1083, doi:10.1175/BAMS-88-7-1059, 2007. 16246

Giorgetta, M. A. and Bengtsson, L.: Potential role of the quasi-biennial oscillation in the stratosphere–troposphere exchange as found in water vapor in general circulation model experiments, J. Geophys. Res., 104, 6003–6019, 1999. 16247, 16248

Giorgetta, M. A., Manzini, E., and Roeckner, E.: Forcing of the quasi-biennial oscillation from a broad spectrum of atmospheric waves, Geophys. Res. Lett., 29, 1245, doi:10.1029/2001GL014756, 2002. 16248

Giorgetta, M. A., Manzini, E., Roeckner, E., Esch, M., and Bengtsson, L.: Climatology and forcing of the quasi-biennial oscillation in the MAECHAM5 model, J. Climate, 19, 3882–3901, 2006. 16248, 16252, 16253

Grainger, R., Lambert, A., Rogers, C., Taylor, F., and Deshler, T.: Straospheric aerosol effective radius, surface area and volume estimated from infrared measurements, J. Geophys. Res., 100, 16507–16518, 1995. 16259

Grant, W., Browell, E. V., Long, C. S., and Stowe, I. I.: Use of volcanic aerosols to study the tropical stratospheric reservoir, J. Geophys. Res., 101, 3973–3988, 1996. 16252, 16253, 16254

Gray, L. J. and Chipperfield, M. P.: On the interannual variability of trace gases in the middle atmosphere, Geophys. Res. Lett., 17, 933–936, 1990. 16246, 16264, 16268

Hamill, P., Jensen, E. J., Russel, P. B., and Bauman, J. J.: The life cycle of stratospheric aerosol particles, B. Am. Meteorol. Soc., 78, 1395–1410, 1997. 16249, 16265, 16266

Hasebe, F.: Quasi-biennial oscillations of ozone and diabatic circulation in the equatorial stratosphere, J. Atmos. Sci., 51, 729–745, 1994. 16256, 16270

Hofmann, D., Barnes, J., O'Neill, M., Trudeau, M., and Neely, R.: Increase in background stratospheric aerosol observed with lidar at Mauna Loa Observatory and Boulder, Colorado., Geophys. Res. Lett., 36, L15808, doi:10.1029/2009GL039008, 2009. 16244, 16245

Hofmann, D. J.: Increase in the stratospheric background sulfuric acid aerosol mass in the past 10 years, Science, 248, 996–1000, 1990. 16245, 16270

Holton, J. R., Haynes, P. H., McIntyre, M. E., Douglass, A. R., Rood, R. R., and Pfister, L.: Stratospheric–tropospheric exchange, Rev. Geophys., 33, 403–439, 1995. 16244

Hommel, R.: Die Variabilität von stratosphärischem Hintergrund-Aerosol. Eine Untersuchung mit dem globalen sektionalen Aerosolmodell MAECHAM5-SAM2, Ph.D. thesis, Universität Hamburg, 2008. 16249

Hommel, R., Timmreck, C., and Graf, H. F.: The global middle-atmosphere aerosol model MAECHAM5-SAM2: comparison with satellite and in-situ observations, Geosci. Model Dev., 4, 809–834, doi:10.5194/gmd-4-809-2011, 2011. 16246, 16280, 16282

Höpfner, M., Glatthor, N., Grabowski, U., Kellmann, S., Kiefer, M., Linden, A., Orphal, J., Stiller, G., von Clarmann, T., Funke, B., and Boone, C. D.: Sulfur dioxide (SO_2) as observed by MIPAS/Envisat: temporal development and spatial distribution at 15–45 km altitude, Atmos. Chem. Phys., 13, 10405–10423, doi:10.5194/acp-13-10405-2013, 2013. 16246, 16267, 16268

IPCC: Climate Change 2013: The Physical Science Basis. Contribution of Working Group I to the Fifth Assessment Report of the Intergovernmental Panel on Climate Change, edited by: Stocker, T. F., Qin, D., Plattner, G.-K., Tignor, M., Allen, S. K., Boschung, J., Nauels, A., Xia, Y., Bex, V., and Midgley, P. M., Cambridge University Press, Cambridge, UK and New York, NY, USA, 1535 pp., 2013. 16246

Title Page

Abstract | Introduction

Conclusions | References

Tables | Figures

◀◀ | ▶▶

◀ | ▶

Back | Close

Full Screen / Esc

Printer-friendly Version

Interactive Discussion

Junge, C. E., Chagnon, C. W., and Manson, J. E.: Stratospheric aerosols, J. Meteorol., 18, 81–108, 1961. 16244

Lin, S. J. and Rood, R. B.: Multidimensional flux form semi-Lagrangian transport, Mon. Weather Rev., 124, 2046–2068, 1996. 16249

5 Manzini, E., Giorgetta, M. A., Esch, M., Kornblueh, L., and Roeckner, E.: The influence of sea surface temperatures on the northern winter stratosphere: ensemble simulations with the MAECHAM5 model, J. Climate, 19, 3863–3881, 2006. 16247

Mills, M., Toon, O. B., and Solomon, S.: A 2-D microphysical model of the polar stratospheric CN layer, Geophys. Res. Lett., 26, 1133–1136, 1999. 16267

10 Mills, M., Toon, O., Vaida, V., Hintze, P., Kjaergaard, H., Schofield, D., and Robinson, T.: Photolysis of sulfuric acid vapor by visible light as a source of the polar stratospheric CN layer, J. Geophys. Res., 110, D08201, doi:10.1029/2004JD005519, 2005. 16267, 16268

Mote, P. W., Rosenlof, K. H., McIntyre, M. E., Carr, E. S., Gille, J. C., Holton, J. R., Kinnersley, J. S., Pumphrey, H. C., Russell III, J. M., and Waters, J. W.: An atmospheric tape

15 recorder: the imprint of tropical tropopause temperatures on stratospheric water vapor, J. Geophys. Res., 101, 3989–4006, 1996. 16253

Naujokat, B.: An update of the observed quasi-biennial oscillation of the stratospheric winds over the tropics, J. Atmos. Sci., 43, 1873–1877, 1986. 16248

Neely, R. R. I., Toon, O. B., Solomon, S., Vernier, J.-P., Alvarez, C., English, J. M.,

20 Rosenlof, K. H., Mills, M. J., Bardeen, C. G., Daniel, J. S., and Thayer, J. P.: Recent anthropogenic increases in SO_2 from Asia have minimal impact on stratospheric aerosol, Geophys. Res. Lett., 40, 1–6, doi:10.1002/grl.50263, 2013. 16245, 16259, 16270

Neu, J. L., Sparling, L. C., and Plumb, R. A.: Variability of the subtropical "edges" in the stratosphere, J. Geophys. Res., 108, 4482, doi:10.1029/2002JD002706, 2003. 16254

25 Niemeier, U., Timmreck, C., Graf, H.-F., Kinne, S., Rast, S., and Self, S.: Initial fate of fine ash and sulfur from large volcanic eruptions, Atmos. Chem. Phys., 9, 9043–9057, doi:10.5194/acp-9-9043-2009, 2009. 16246

Pitari, G., Mancini, E., Rizi, V., and Shindell, D. T.: Impact of future climate and emission changes on stratospheric aerosols and ozone, J. Atmos. Sci., 59, 414–440, 2002. 16246

30 Plumb, R. A. and Bell, R. C.: A model of quasibiennial oscillation on an equatorial beta-plane, Q. J. Roy. Meteor. Soc., 108, 335–352, 1982. 16254

Rex, M., Timmreck, C., Kremser, S., Thomason, L., and Vernier, J.-P.: Stratospheric sulphur and its role in climate (SSiRC), in: SPARC Newsletter 39, p. 37, WMO/SPARC, Zurich, 2012. 16245

Rinsland, C. P., Gunson, M. R., Ko, M. K. W., Weisenstein, D. W., Zander, R., Abrams, M. C., Goldman, A., Sze, N. D., and Yue, G. K.: H_2SO_4 photolysis: a source of sulfur dioxide in the upper stratosphere, Geophys. Res. Lett., 22, 1109–1112, 1995. 16246, 16267

Roeckner, E., Baeuml, G., Bonaventura, L., Brokopf, R., Esch, M., Giorgetta, M., Hagemann, S., Kirchner, I., Kornblueh, L., Manzini, E., Rhodin, A., Schlese, U., Schulzweida, U., and Tompkins, A.: The atmospheric general circulation model ECHAM5 – Part I, Max Planck Institute for Meteorology, Hamburg, Germany, MPI Report No. 349, 2003. 16249

Rosen, J. M.: The boiling point of stratospheric aerosols, J. Applied Meteor., 10, 1044–1045, 1971. 16265, 16289

Sander, S., Friedl, R., Ravishankara, A., Golden, D., Kolb, C., Kurylo, M., Huie, R., Orkin, V., Molina, M., Moortgat, G., and Finlayson-Pitts, B.: Chemical Kinetics and Photochemical Data for Use in Atmospheric Studies, JPL Publication 06-2, Evaluation No 15, NASA Jet Propulsion Laboratory, California Institute of Technology, Pasadena, California, 2006. 16269

Seinfeld, J. H. and Pandis, S. N.: Atmospheric Chemistry and Physics: From Air Pollution to Climate Change, 2nd edn., Wiley-Interscience, New York, 2006. 16260

Seol, D.-I. and Yamazaki, K.: QBO and Pinatubo signals in the mass flux at 100 hPa and stratospheric circulation, Geophys. Res. Lett., 25, 1641–1644, 1998. 16264, 16268

Solomon, S., Daniel, J. S., Neely, R. R., Vernier, J.-P., Dutton, E. G., and Thomason, L. W.: The persistently variable "background" stratospheric aerosol layer and global climate change, Science, 333, 866–870, doi:10.1126/science.1206027, 2011. 16245, 16270

SPARC/ASAP: WMO/SPARC Scientific Assessment of Stratospheric Aerosol Properties (ASAP), WCRP-124 WMO/TD- No. 1295, SPARC Report No. 4, edited by: Thomason, L. and Peter, T., WMO, 2006. 16244, 16245, 16246, 16247, 16251, 16257, 16258, 16267

Steele, H. M. and Hamill, P.: Effects of temperature and humidity on the growth and optical properties of sulfuric acid–water droplets in the stratosphere, J. Aerosol Sci., 12, 517–528, 1981. 16266

Stier, P., Feichter, J., Kinne, S., Kloster, S., Vignati, E., Wilson, J., Ganzeveld, L., Tegen, I., Werner, M., Balkanski, Y., Schulz, M., Boucher, O., Minikin, A., and Petzold, A.: The aerosol-climate model ECHAM5-HAM, Atmos. Chem. Phys., 5, 1125–1156, doi:10.5194/acp-5-1125-2005, 2005. 16249

Title Page

Abstract | Introduction

Conclusions | References

Tables | Figures

|◄ | ►|

◄ | ►

Back | Close

Full Screen / Esc

Printer-friendly Version

Interactive Discussion

The Royal Society, Geoengineering in Climate: Science, Governance and Uncertainty, RS Policy Report 10/09, The Royal Society, London, ISBN 978-0-85403-773-5, 2009. 16245

Thomason, L. W., Burton, S. P., Luo, B.-P., and Peter, T.: SAGE II measurements of stratospheric aerosol properties at non-volcanic levels, Atmos. Chem. Phys., 8, 983–995, doi:10.5194/acp-8-983-2008, 2008. 16245, 16256

Timmreck, C.: Three-dimensional simulation of stratospheric background aerosol: first results of a multiannual general circulation model simulation, J. Geophys. Res., 106, 28313–28332, 2001. 16246

Trepte, C. R. and Hitchman, M. H.: Tropical stratospheric circulation deduced from satellite aerosol data, Nature, 355, 626–628, 1992. 16252, 16253, 16254, 16269

Turco, R. P., Hamill, P., Toon, O. B., Whitten, R. C., and Kiang, C. S.: A one-dimensional model describing aerosol formation and evolution in the stratosphere: I. physical processes and mathematical analogs, J. Atmos. Sci., 36, 699–717, 1979. 16268

Vehkamäki, H., Kulmala, M., Napari, I., Lehtinen, K. E. J., Timmreck, C., Noppel, M., and Laaksonen, A.: An improved parameterization for sulfuric acid water nucleation rates for tropospheric and stratospheric conditions, J. Geophys. Res., 107, 4622–4632, 2002. 16249, 16263, 16288

Vernier, J.-P., Thomason, L. W., Pommereau, J.-P., Bourassa, A., Pelon, J., Garnier, A., Hauchecorne, A., Blanot, L., Trepte, C., Degenstein, D., and Vargas, F.: Major influence of tropical volcanic eruptions on the stratospheric aerosol layer during the last decade, Geophys. Res. Lett., 38, L12807, doi:10.1029/2011GL047563, 2011. 16259

Weisenstein, D. K., Yue, G. K., Ko, M. K. W., Sze, N.-D., Rodriguez, J. M., and Scott, C. J.: A two-dimensional model of sulfur species and aerosols, J. Geophys. Res., 102, 13019–13035, 1997. 16268

Wurl, D., Grainger, R. G., McDonald, A. J., and Deshler, T.: Optimal estimation retrieval of aerosol microphysical properties from SAGE II satellite observations in the volcanically unperturbed lower stratosphere, Atmos. Chem. Phys., 10, 4295–4317, doi:10.5194/acp-10-4295-2010, 2010. 16250, 16251, 16258

Yue, G., Poole, L., Wang, P.-H., and Chiou, E.: Stratospheric aerosol acidity, density, and refractive index deduced from SAGE II and NMC temperature data, J. Geophys. Res., 99, 3727–3738, 1994. 16266

The QBO in tropical stratospheric aerosol

R. Hommel et al.

Title Page

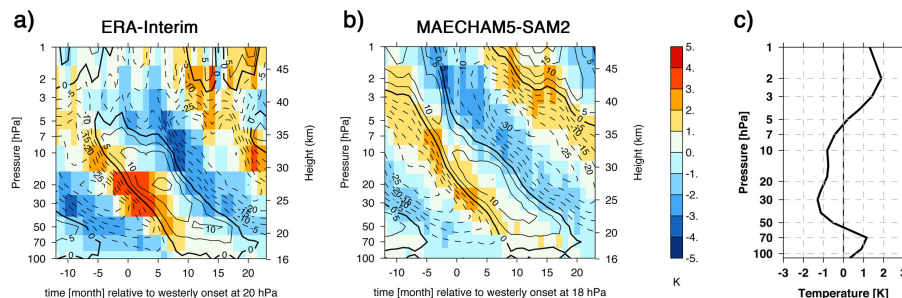| Abstract | Introduction |
| Conclusions | References |
| Tables | Figures |

|◄ | ►|

◄ | ►

Back | Close

Full Screen / Esc

Printer-friendly Version

Interactive Discussion

Table A1. Abbreviations.

AMIP2	Atmospheric Model Intercomparison Project
ASAP	Assessment of Stratospheric Aerosol Properties
ATMOS	Atmospheric Trace Molecule Spectroscopy
BDC	Brewer–Dobson Circulation
BHN	Binary Homogeneous Nucleation
CALIOP	Cloud-Aerosol Lidar with Orthogonal Polarisation
CCM	Chemistry Climate Model
CCMI	Chemistry-Climate Model Initiative
CCMVal	Chemistry-Climate Model Validation Activity
CTL	Control (experiment)
ECHAM	Acronym from ECMWF and Hamburg
ECMWF	European Centre for Medium Range Weather Forecasts
ERA	ECMWF Re-Analysis
ERBS	Earth Radiation Budget Satellite
HALOE	Halogen Occultation Experiment
QBO	Quasi-Biennial Oscillation
MIPAS	Michelson Interferometer for Passive Atmospheric Sounding
NASA	National Aeronautics and Space Administration
SAD	Surface Area Density
SAGE	Stratospheric Aerosol and Gas Experiment
SAM2	Stratospheric Aerosol Model version 2
SAO	Semi-Annual Oscillation
SMC	Secondary Meridional Circulation
SOLVE	SAGE III Ozone Loss and Validation Experiment
SPARC	Stratospheric Processes and their Role in Climate
TSR	Tropical Stratospheric Reservoir
TTL	Tropical Tropopause Layer
UT/LS	Upper troposphere and Lower Stratosphere
WMO	World Meteorological Organisation

Title Page

Abstract | Introduction

Conclusions | References

Tables | Figures

|◄ | ►|

◄ | ►

Back | Close

Full Screen / Esc

Printer-friendly Version

Interactive Discussion
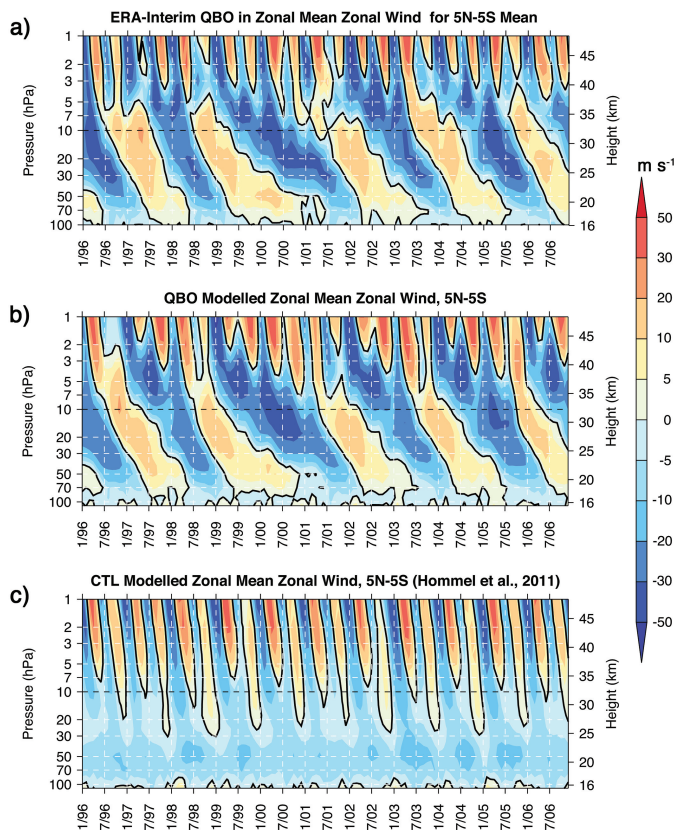
Figure 1. Temporal evolution of the monthly zonal mean zonal wind in the equatorial lower stratosphere between 5° N and 5° S for the years 1996–2006 in the **(a)** ECMWF ERA-Interim reanalysis and MAECHAM5-SAM2 simulations **(b)** with QBO-nudging and **(c)** in the control experiment (CTL) of Hommel et al. (2011). Reddish colours represent westerlies, blueish easterlies. Black countours highlights the month and altitude of wind transition.

Figure 2. Residual temperature anomalies induced by the QBO in **(a)** the ERA-Interim reanalysis and **(b)** the QBO-nudged MAECHAM5-SAM2 simulation between 5° N and 5° S. Composited for the years 1996–2006 relative to the onset of residual westerlies at 20 hPa and 18 hPa, respectively. Black contours denote the residual zonal mean zonal wind, where dashed lines represent easterlies. Contour interval is $5\,\mathrm{m\,s^{-1}}$. The difference between the climatological averaged temperature profiles of the QBO-nudged simulation and the control experiment (QBO-CTL) is shown in **(c)**.
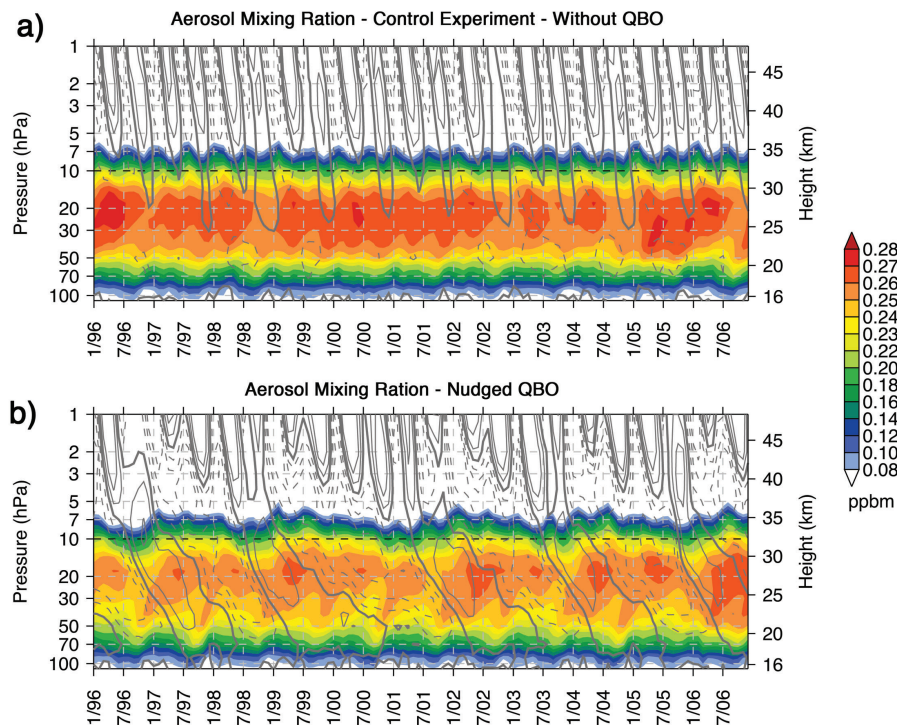
Figure 3. Temporal evolution of the monthly mean zonal mean aerosol mass mixing ratio (kg(S) kg^{-1}) in **(a)** the CTL simulation of Hommel et al. (2011) and **(b)** the QBO-nudged model between 5° N and 5° S for the years 1996–2006. Gray contours denote the zonal wind as in Fig. 1, where dashed lines represent easterlies.

Discussion Paper | Discussion Paper | Discussion Paper | Discussion Paper |

ACPD

14, 16243–16290, 2014

The QBO in tropical stratospheric aerosol

R. Hommel et al.

Title Page

Abstract	Introduction
Conclusions	References
Tables	Figures

|◄ ►|

◄ ►

Back Close

Full Screen / Esc

Printer-friendly Version

Interactive Discussion
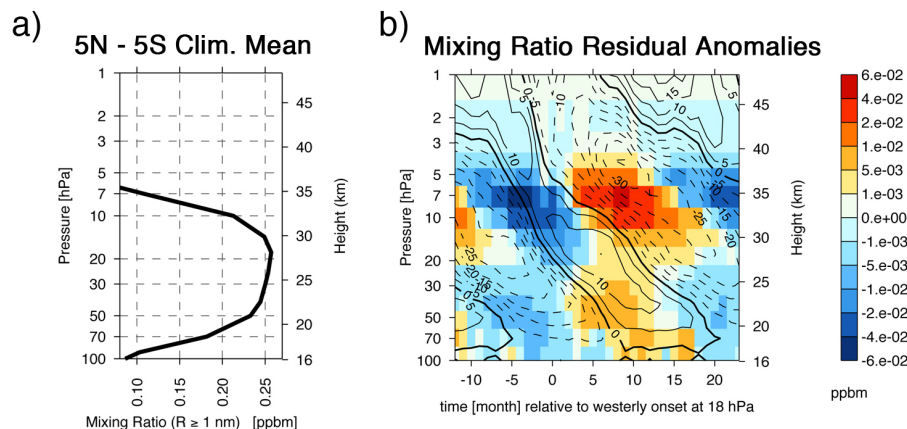
Figure 4. Climatological mean profile of the modelled aerosol mass mixing ratio between 5° N and 5° S for the period 1996–2006. **(b)** Composite of QBO induced residual anomalies in the modelled aerosol mass mixing ratio with respect to the time of onset of westerly zonal mean zonal wind at 18 hPa. As in Fig. 2b, black contours denote the residual zonal wind. Dashed lines represent easterlies, contour interval is $5\,\mathrm{m\,s^{-1}}$.
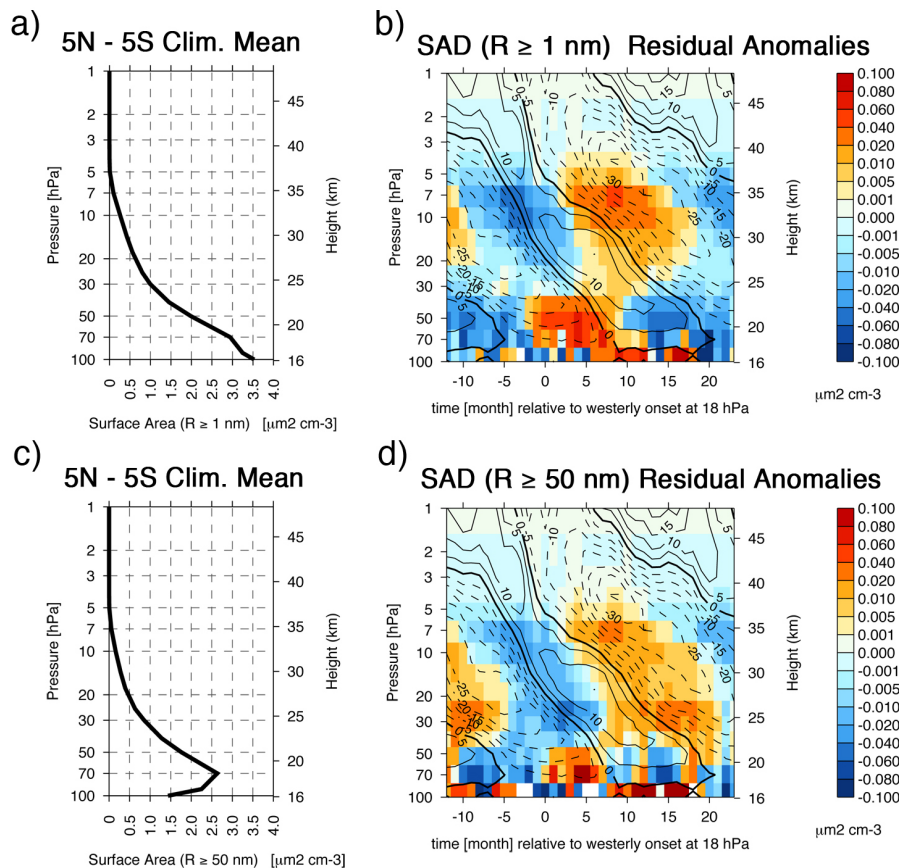
Figure 5. As in Fig. 4, except for residual anomalies in the aerosol surface area density (SAD). Upper panel inferred from the entire size distribution $1\,\mathrm{nm} \le R < 2.6\,\mu\mathrm{m}$, lower panel for aerosols with $R \ge 50\,\mathrm{nm}$.

Title Page

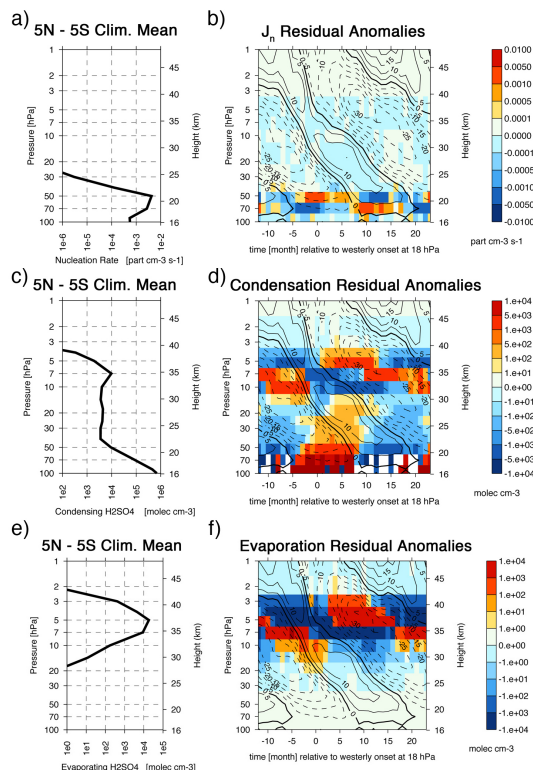Abstract | Introduction

Conclusions | References

Tables | Figures

|◄ | ►|

◄ | ►

Back | Close

Full Screen / Esc

Printer-friendly Version

Interactive Discussion
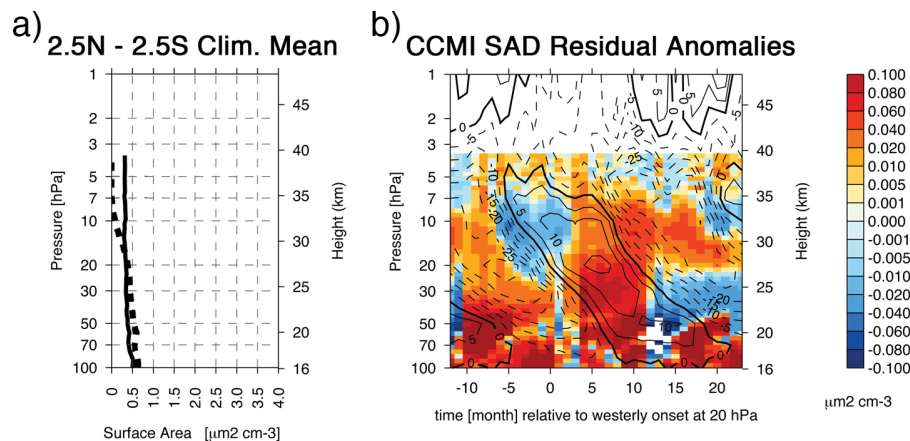
Figure 6. As in Fig. 4, except for the SAD climatology between 2.5° N and 2.5° S of the SPARC CCMI initiative, inferred from spaceborne SAGE II and CALIOP observations. The profile in **(a)** is complemented by the climatological averaged SAD of the SPARC CCMVal initiative. The overlaid zonal wind in **(b)** is obtained from the ECMWF ERA-Interim climatology as in Fig. 2a.
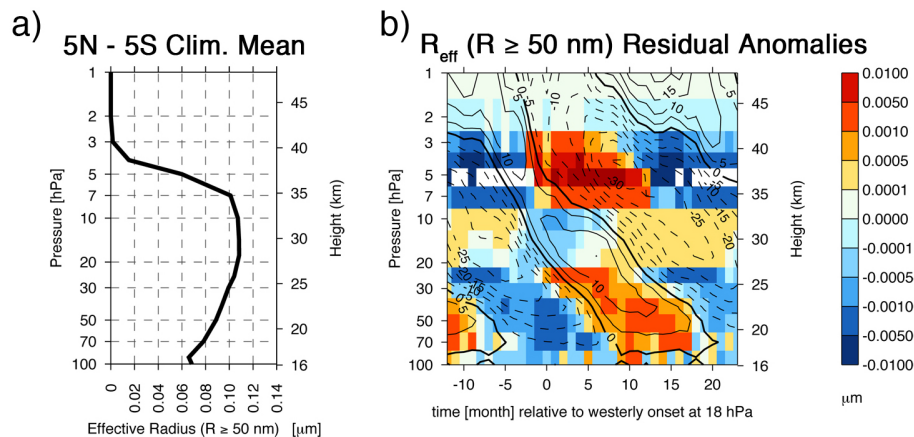
Figure 7. As in Fig. 4, except for the effective radius of aerosols with $R \geq 50\,\text{nm}$.
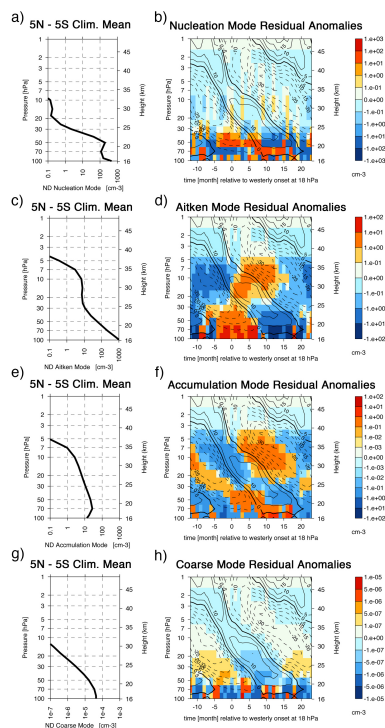
Figure 8. As in Fig. 4, except for modelled number densities as integrals over specified modes: **(a)** and **(b)** nucleation mode ($R < 0.005\,\mu m$), **(c)** and **(d)** Aitken mode ($0.005\,\mu m \leq R < 0.05\,\mu m$), **(e)** and **(f)** accumulation mode ($0.05\,\mu m \leq R < 0.5\,\mu m$), and **(g)** and **(h)** coarse mode ($R \geq 0.5\,\mu m$).

Figure 9. As in Fig. 4, except for modelled microphysical processes. The upper panel shows the binary homogeneous nucleation rate ($cm^{-3} s^{-1}$) as parametrised by Vehkamäki et al. (2002), the middle panel the time-averaged H_2SO_4 vapour concentration (cm^{-3}) that condenses onto aerosols. The bottom panel shows the time-averaged H_2SO_4 vapour concentration (cm^{-3}) that evaporats from aerosols.
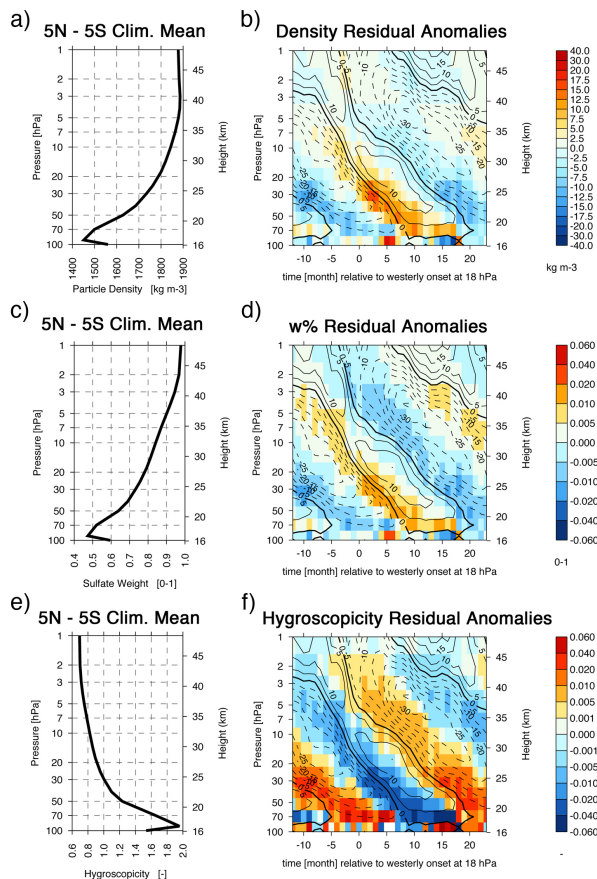
Figure 10. As in Fig. 4, except for modelled sulphate aerosol properties. The upper panel shows the density of the binary H_2SO_4–H_2O solution, the middle panel the H_2SO_4 weight percentage, and the bottom panel the aerosol water content relative to a representative Junge layer aerosol composition (e.g. Rosen, 1971).

Title Page

Abstract | Introduction

Conclusions | References

Tables | Figures

|◄ | ►|

◄ | ►

Back | Close

Full Screen / Esc

Printer-friendly Version

Interactive Discussion
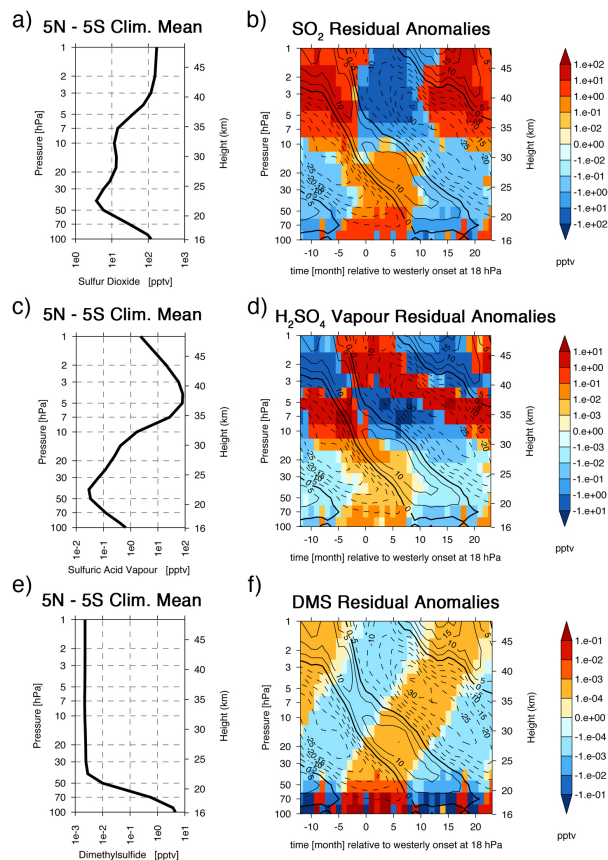
Figure 11. As in Fig. 4, except for prognostic sulphate aerosol precursor gases. The upper panel shows the SO_2 mass mixing ratio, the middle panel the H_2SO_4 mass mixing ratio, and the bottom panel the DMS mass mixing ratio.